Am J Nucl Med Mol Imaging 2014;4(3):248-259
www.ajnmmi.us /ISSN:2160-8407/ajnmmi1401006

Original Article

Automated synthesis and dosimetry of 6-deoxy-6-[^{18}F]fluoro-D-fructose (6-[^{18}F]FDF): a radiotracer for imaging of GLUT5 in breast cancer

Vincent Bouvet[1], Hans S Jans[1], Melinda Wuest[1], Olivier-Mohamad Soueidan[2], John Mercer[1], Alexander JB McEwan[1], Frederick G West[2], Chris I Cheeseman[3], Frank Wuest[1]

Departments of [1]Oncology, [2]Chemistry, [3]Physiology, University of Alberta, Edmonton, AB – T6G 1Z2, Canada

Received January 16, 2014; Accepted February 7, 2014; Epub April 25, 2014; Published April 30, 2014

Abstract: 6-Deoxy-6-[^{18}F]fluoro-D-fructose (6-[^{18}F]FDF) is a promising PET radiotracer for imaging GLUT5 in breast cancer. The present work describes GMP synthesis of 6-[^{18}F]FDF in an automated synthesis unit (ASU) and dosimetry calculations to determine radiation doses in humans. GMP synthesis and dosimetry calculations are important prerequisites for first-in-human clinical studies of 6-[^{18}F]FDF. The radiochemical synthesis of 6-[^{18}F]FDF was optimized and adapted to an automated synthesis process using a Tracerlab FX_{FN} ASU (GE Healthcare). Starting from 30 GBq of cyclotron-produced n.c.a. [^{18}F]fluoride, 2.9 ± 0.1 GBq of 6-[^{18}F]FDF could be prepared within 50 min including HPLC purification resulting in an overall decay-corrected radiochemical yield of 14 ± 3% (n = 11). Radiochemical purity exceeded 95%, and the specific activity was greater than 5.1 GBq/μmol. Sprague-Dawley rats were used for biodistribution experiments, and dynamic and static small animal PET experiments. Biodistribution studies served as basis for allometric extrapolation to the standard man anatomic model and normal organ-absorbed dose calculations using OLINDA/EXM software. The calculated human effective dose for 6-[^{18}F]FDF was 0.0089 mSv/MBq. Highest organ doses with a dose equivalent of 0.0315 mSv/MBq in a humans were found in bone. Injection of 370 MBq (10 mCi) of 6-[^{18}F]FDF results in an effective whole body radiation dose of 3.3 mSv in humans, a value comparable to that of other ^{18}F-labeled PET radiopharmaceuticals. The optimized automated synthesis under GMP conditions, the good radiochemical yield and the favorable human radiation dosimetry estimates support application of 6-[^{18}F]FDF in clinical trials for molecular imaging of GLUT5 in breast cancer patients.

Keywords: Positron emission tomography, automated synthesis, dosimetry, 6-[^{18}F]FDF, GLUT5

Introduction

Breast cancer is the most frequently diagnosed malignancy in women worldwide [1]. Various non-invasive molecular imaging technologies have significantly advanced diagnosis and monitoring of treatment efficacy of cancer. Among molecular imaging methodologies, positron emission tomography (PET) represents one of most sensitive techniques for functional molecular imaging of malignancies *in vivo* [2]. The most widely used PET radiotracer for molecular imaging of tumor metabolism and monitoring of disease management in breast cancer is 2-deoxy-2-[^{18}F]fluoro-D-glucose ([^{18}F]FDG) [3]. Although [^{18}F]FDG-PET has been used in numerous clinical studies with breast cancer patients, it has shown several limitations based on its variable sensitivity and specificity. According to current National Comprehensive Cancer Network (NCCN) guidelines, [^{18}F]FDG-PET does not have a role in breast cancer screening. Moreover, the sensitivity of [^{18}F]FDG-PET in detecting primary breast cancer is less than other imaging modalities, limiting its usefulness in routine screening and lymph node staging of breast cancer [4].

Deregulation of energy metabolism of tumor cells is associated with an increased rate of glycolysis resulting in higher uptake and phosphorylation of glucose [5]. However, analysis of facilitative hexose transporter 1 (GLUT1) expression in different types of human cancers, including breast cancer, revealed a GLUT1 expression in only 46 to 67% of the samples.

This study indicates that a rather large population (30 to almost 50%) of breast cancer patients exhibit only very low or no GLUT1 expression levels [6-8]. This fact may account for the low or no uptake of [18F]FDG in these patients.

Besides [18F]FDG, other PET radiotracers such as the proliferation marker 3'-deoxy-3'-[18F]fluorothymidine ([18F]FLT), the estrogen receptor (ER)-binding ligand 16α-[18F]fluoro-17β-estradiol ([18F]FES), the progesterone receptor (PR)-binding 18F-labeled progestins such as 21-[18F]fluoro-16α-ethyl-19-norprogesterone ([18F]FENP) and the more recently developed 4-[18F]fluoropropyl-tanaproget ([18F]FPTP) have been used for functional imaging in breast cancer patients [9-12].

Steroid hormone receptor-binding radiotracers offer the opportunity to predict breast cancer patients' response to anti-hormonal therapy. However, they are not diagnostic in ER and PR negative breast cancer patients.

Fructose metabolism is an alternative energy metabolism to glycolysis in breast cancer. Fructose metabolism is initiated through transport of fructose via facilitative hexose transporter GLUT5 [13]. Elevated levels of GLUT5 expression have been found in several types of cancer including breast cancer [14]. Imaging employing GLUT5-mediated fructose uptake would allow targeting of an alternative metabolic pathway independent of the main glucose transporter GLUT1. Targeting GLUT5 would be a feasible approach for GLUT1 negative and [18F]FDG silent breast cancer patients. However, there is still an ongoing debate on the extent of GLUT5 expression in breast cancer tissue, and its relevance as a diagnostic target in breast cancer patients [15].

Very little is currently known about the status of GLUT1 and GLUT5 expression in breast cancer patients and their correlation with hormone receptor status and energy metabolism.

Recently developed molecular probes, including radiotracers, for imaging GLUT5 in breast cancer include 1-deoxy-1-[18F]fluoro-D-fructose (1-[18F]FDF, [16]), cyclic furanose analogues [17, 18], and 6-deoxy-6-[18F]fluoro-D-fructose (6-[18F]FDF [19, 20]). 6-[18F]FDF showed GLUT5-mediated uptake *in vitro* and *in vivo* in various murine and human breast cancer cell lines. Radiopharmacological evaluation of 6-[18F]FDF including small animal PET studies demonstrated the feasibility of the radiotracer for molecular imaging of GLUT5 in breast cancer [20].

The goal of the present work was the establishment of an automated synthesis of 6-[18F]FDF in an ASU according to GMP guidelines and calculation of absorbed radiation dose in humans as prerequisites for initiation of a clinical trial with 6-[18F]FDF in breast cancer patients.

Materials and methods

Synthesis of methyl 1,3,4-tri-O-acetyl-6-O-tosyl-α-D-fructofuranoside

Methyl 1,3,4-tri-*O*-acetyl-α-D-fructofuranoside (64 mg, 0.2 mmol) was dissolved in pyridine (0.4 mL) at room temperature. 4-Methylbenzenesulfonyl chloride (0.22 mmol) was then added in a single portion. The reaction mixture was allowed to stir for 24 hours before the addition of water (5 mL) and CH_2Cl_2 (5 mL). Upon separation of the organic/aqueous layers, the organic layer was washed with 10% H_2SO_4 aq. (2 x 5 mL) and saturated $NaHCO_3$ solution (5 mL). The organic layer was then dried ($MgSO_4$) and filtered before removal of the solvent in vacuo. The crude material was subjected to purification by column chromatography (7:3, EtOAc:hexanes, silica gel) to afford pure methyl 1,3,4-tri-*O*-acetyl-6-*O*-tosyl-α-D-fructofuranoside (0.1 mmol, 67%). R_f 0.50 (hexanes/EtOAc 3:7); IR (thin film) 2960, 1748, 1598, 1369, 1230, 1190, 1093 cm-1; 1H-NMR (400 MHz, $CDCl_3$) δ 7.80 (d, J = 8.4 Hz, 2H), 7.35 (d, J = 8.4 Hz, 2H), 5.46 (d, J = 6.8 Hz, 1H), 5.25 (dd, J = 6.0, 7.2 Hz, 1H), 4.29 (dd, J = 3.2, 10.0 Hz, 1H), 4.21 (d, J = 12.0 Hz, 1H), 4.16 (ddd, J = 3.2, 5.6, 7.2 Hz, 1H), 4.13 (d, J = 12.0 Hz, 1H), 4.09 (dd, J = 7.6, 10.4 Hz, 1H), 3.23 (s, 3H), 2.45 (s, 3H), 2.09 (s, 3H), 2.08 (s, 3H), 2.05 (s, 3H); 13C-NMR (100 MHz, CDCl3) δ 170.2, 170.0, 169.8, 145.0, 132.6, 129.9, 128.0, 103.1, 77.9, 76.0, 75.7, 69.5, 61.7, 49.7, 21.6, 20.7, 20.6, 20.6. HRMS (EI, [M+Na]+) for $C_{20}H_{26}NaO_{11}S$ calcd 497.1088, found: m/z 497.1078.

Production of [18F]fluoride

[18F]fluoride was produced by the $^{18}O(p,n)^{18}F$ nuclear reaction through proton irradiation of enriched (98%) [18O]water (3.0 mL, Rotem,

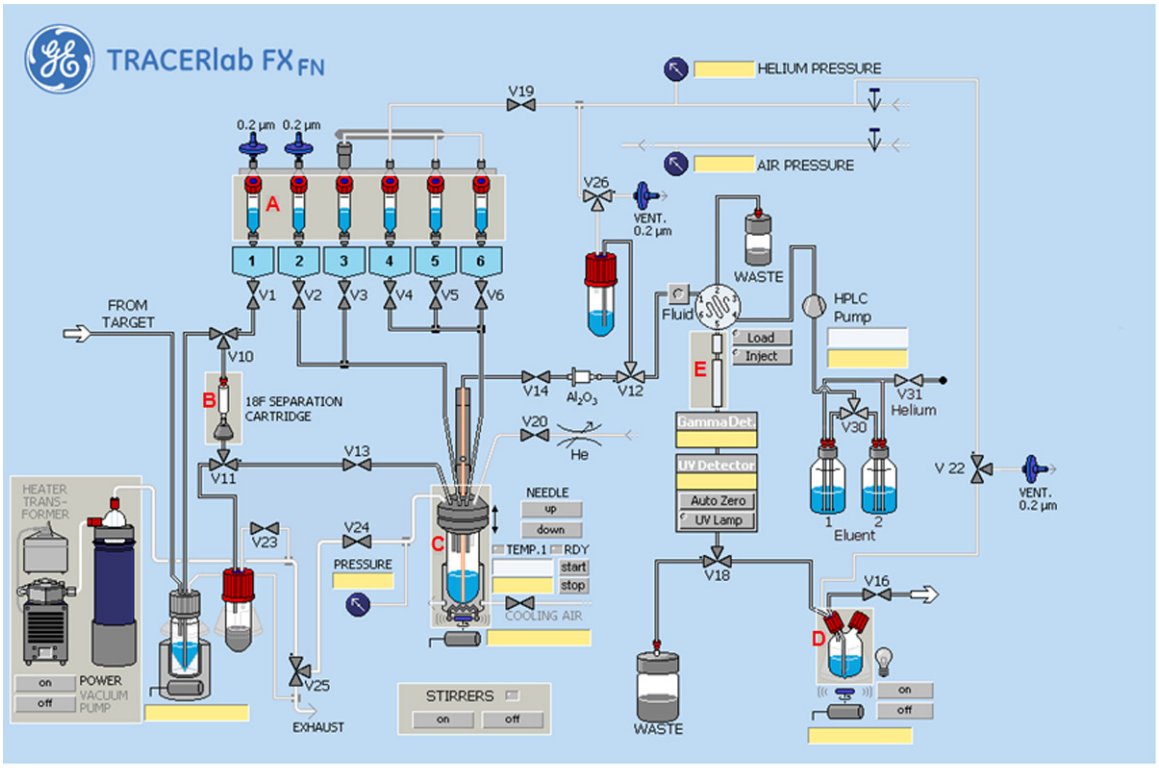

A: Reactant reservoirs
B: ^{18}F Separation cartridges
C: Reactor
D: Product collecting vial
E: Purification columns

V1: K_2CO_3/ $K_{2.2.2}$ (0.8 mL)
V2: anhydrous CH_3CN (1 mL)
V3: FDF precursor (7-14 mg in 0.5 mL CH_3CN)
V4: 2N HCl (1 mL)
V5: H_2O (1 mL)
V6: Rinse SWFI (2 mL)

Figure 1. Scheme of automated synthesis unit for radiosynthesis of 6-[^{18}F]FDF.

Germany) using a TR19/9 cyclotron (Advanced Cyclotron systems Inc., Richmond, British Columbia, Canada).

Automated synthesis of 6-[^{18}F]FDF

6-Deoxy-6-[^{18}F]fluoro-D-fructose (6-[^{18}F]FDF) was synthesized according to a modified procedure previously published by our group [20]. Instead of using the reported triflate precursor, in this study we used corresponding tosylate compound as the labeling precursor. Radiosynthesis of 6-[^{18}F]FDF was performed on a GE TRACERlab™ FX (GE Healthcare, Mississauga, Ontario, Canada). The ASU was modified in terms of program and hardware (**Figure 1**).

The ASU was installed and operated in a shielded hot cell. The synthesis unit was equipped with an integrated HPLC system using a Phenomenex Nucleosil LUNA (II) RP C18 pre-column (5 µm, 50 x 10 mm) and Phenomenex Nucleosil LUNA C18 column (10 µm, 250 x 10 mm; Torrence, CA, U.S.A.). The HPLC injection system included a 5 mL loop and the sample was eluted using a 0.1 M sodium acetate buffer (pH = 5.4) solution at 2 mL/min. Radioactivity and UV detectors were incorporated in the base unit and the wavelength was recorded at 240 nm. Radio-TLC was performed on EMD Merck F254 silica gel 60 aluminum-backed TLC plates (EMD Millipore, Billerica, MA, U.S.A.). Radioactivity was detected using the ASU radiodetector (GE Healthcare, Mississauga, Ontario, Canada) during the radiosynthesis, a well-scintillation NaI (Tl) detector, and a Bioscan AR-2000 (Bioscan Inc., Washington DC, U.S.A.) for TLC plate reading. The potassium carbonate and Kryptofix 2.2.2 solutions as well as acetonitrile were purchased from Rotem Industries Ltd (Durham, NC, U.S.A.), sodium acetate and

glacial acetic acid from Sigma Aldrich (St. Louis, MO, U.S.A.), HCl from Huayi Isotopes Canada (Toronto, Ontario, Canada).

Sterile water for injection (SWFI) was obtained from Hospira Healthcare Corp. (St. Laurent, Quebec, Canada). ^{18}F Separation cartridges (Chromafix Strong PS-DVB^{-}) Ion exchange in HCO_3^- form were purchased from Machery-Nagel (MACHEREY-NAGEL GmbH & Co. KG, Dueren, Germany), Alumina N cartridges from Waters (Milford, MA, U.S.A.), Millex HV outlet filters from Millipore (EMD Millipore, Billerica, MA, U.S.A.), Chemovent vent filters from IMI Int. Medical Industries (Pompano Beach, Fl, U.S.A.), and 20 mL sterile collecting vials from Mallinckrodt (St. Louis, Mo, U.S.A.).

Animal model

All animal experiments were carried out in accordance with the guidelines of the Canadian Council on Animal Care (CCAC) and were approved by the local animal care committee of the Cross Cancer Institute. Imaging and biodistribution studies were carried out with adult female Sprague-Dawley rats (Charles-River, Canada).

Small animal PET imaging

Rats were injected with 12-17 MBq of 6-[^{18}F]FDF in saline (150 to 200 μL). Accurately administered activity was calculated as the difference between syringe activity before and after injection; activities were determined in a dose calibrator (Atomlab 300, Biodex Medical Systems, Shirley, NY, USA). Rats were anesthetized through inhalation of isoflurane in 40% oxygen/60% nitrogen (gas flow, 1 L/min), and body temperature was kept constant at 37°C for the entire experiment. Rats were positioned and immobilized in the prone position with their medial axis parallel to the central axis of the microPET R4 scanner (Siemens Preclinical Solutions, Knoxville, TN, USA). Dynamic emission scans were performed for 4 h post injection. After a delay of approximately 15 s following the initiation of the scanning sequence, 12-17 MBq of 6-[^{18}F]FDF in 150-200 μl of saline was injected through a needle catheter into the tail vein. Data acquisition continued for 60 min in 3D list mode.

List mode data were sorted into sinograms with 72 time frames (10 x 2 s, 8 x 5 s, 6 x 10 s, 8 x 20 s, 8 x 60 s, 10 x 120 s, 6 x 300 s, 18 x 600 s). The frames were reconstructed using the Ordered Subset Expectation Maximization applied to the 2D sinograms (2D OSEM) and maximum a posteriori (MAP) image reconstruction. Prior to the radiotracer injection, transmission data for the purpose of attenuation correction was acquired using a Co-57 point source. The image files were further processed using the ROVER v2.0.51 software (ABX GmbH). Masks for defining 3D regions of interest (ROI) over tumors and the muscle tissue on the contralateral axilla were set and the ROIs were defined by thresholding. ROI time-activity curves (TACs) were generated for subsequent data analysis.

Standardized uptake values (SUV = [activity/mL tissue] / [injected activity/body weight]) were calculated for each ROI.

Biodistribution experiments

After intravenous injection of 1.5-4 MBq of 6-[^{18}F]FDF in saline (150 to 350 μL) into the tail vein of isoflurane-anesthetized rats, animals were allowed to regain consciousness until sacrifice. While under isoflurane anesthesia, animals were euthanized by decapitation at 5 and 30 min, 1 h, 2 h, 3 h, 4 h, and 6 h post injection and rapidly dissected. Organs of interest including blood, heart, lung, liver, kidneys, thymus, spleen, duodenum, small and large intestine, pancreas, right femur, muscle, stomach, ovaries, brain, fat and bladder were collected and weighed. Radioactivity in all tissues was measured in a γ-counter and results were analyzed as percentage of injected dose per gram of tissue (%ID/g).

Radiation dosimetry analysis

Radiation dosimetry analysis for the determination of the normal organ-absorbed doses and the effective dose was performed using OLINDA/EXM software (version 1.1, Vanderbilt University, Nashville, TN, U.S.A.).

Scaling of the animal-obtained values to human values was carried out by weighting the organ uptake with the relative organ mass in the animal and human:

$$\left(\frac{\%ID}{organ}\right)_{human} = \left(\frac{\%ID}{organ}\right)_{rat} \cdot \left[\left(\frac{m_{organ}}{m_{body}}\right)_{human} \Big/ \left(\frac{m_{organ}}{m_{body}}\right)_{rat}\right] \quad (1)$$

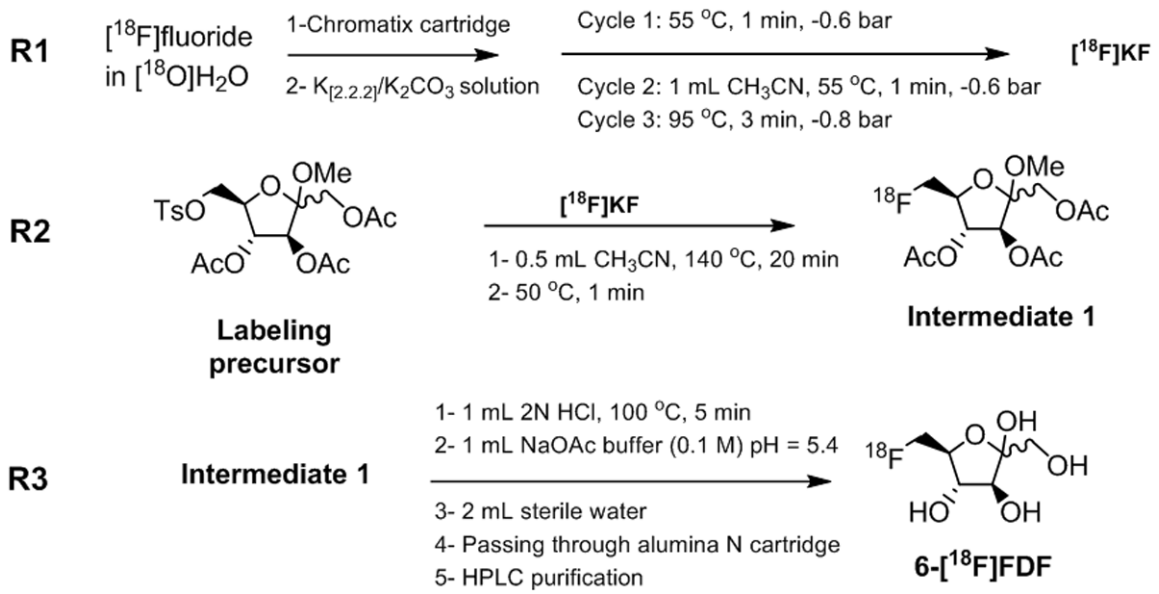

Figure 2. Radiosynthesis of 6-[18F]FDF.

In practice, concentrations $\left(\frac{\%ID}{organ}\right)_{rat} / (m_{organ})_{rat} \equiv \left(\frac{\%ID}{m_{organ}}\right)_{rat}$ are determined experimentally.

This also accounts for organs that cannot be excised in their entirety, such as muscle, blood and bone. **Equation 1** then becomes

$$\left(\frac{\%ID}{m_{organ}}\right)_{human} = \left(\frac{\%ID}{m_{organ}}\right)_{rat} \cdot \frac{(m_{body})_{rat}}{(m_{body})_{human}} \quad (2)$$

The values for $(\%ID/m_{organ})_{human}$ are obtained by first averaging the values $(\%ID/m_{organ})_{rat} \cdot (m_{body})_{rat}$ for the three individual animals sacrificed at each time point and then dividing by the weight of the adult human of 73.7 kg [23, 24]. To obtain the cumulated activity in each organ, these curves were multiplied by the human organ mass, using the values implemented in the OLINDA/EXM code [23], and integrated: for the first 6 hours numerically by evaluating the area under the measured curve and beyond 6 hours by fitting a mono-exponential function to the last four data points of each curve and integrating it from 6 h to infinity.

Not in all cases did the organs for which cumulated activity was determined by means of the biodistribution (see above) correspond to the source organs as defined in OLINDA/EXM. The following assumptions were made to derive the cumulated activity for the OLINDA-defined source organs: (i) It was assumed that all activity detected in the stomach, intestines and the urinary bladder originated from their contents. (ii) Since lower large intestine (LLI) and upper large intestine (ULI) were not measured separately, the measured total activity was distributed to LLI and ULI activity according their mass ratio, using the masses for LLI and ULI walls as defined in the OLINDA/EXM code.

(iii) Since exact quantities of the small amounts of bone and muscle activity contained in the remainder of the body were unknown, they were not subtracted from the whole body activity. (iv) The activity of the heart's content was determined from the blood concentration (decays/mL) and multiplied by the internal volume of the heart (510 mL, ICRP89). (v) It was assumed that activity is uniformly distributed to cortical and trabecular bone and red marrow. The number of decays in each is assigned according to their weight ratio, based on the weight of the human skeleton of 10.45 kg (ICRP89), the ratio of cortical to trabecular bone of 4/1 and the fact that red marrow constitutes 4% of the total body mass [24, 25].

The values determined for cumulated activity in each source organ were then used as input for the OLINDA/EXM code.

Statistics

Biodistribution experiments were repeated with three animals at each time point and the

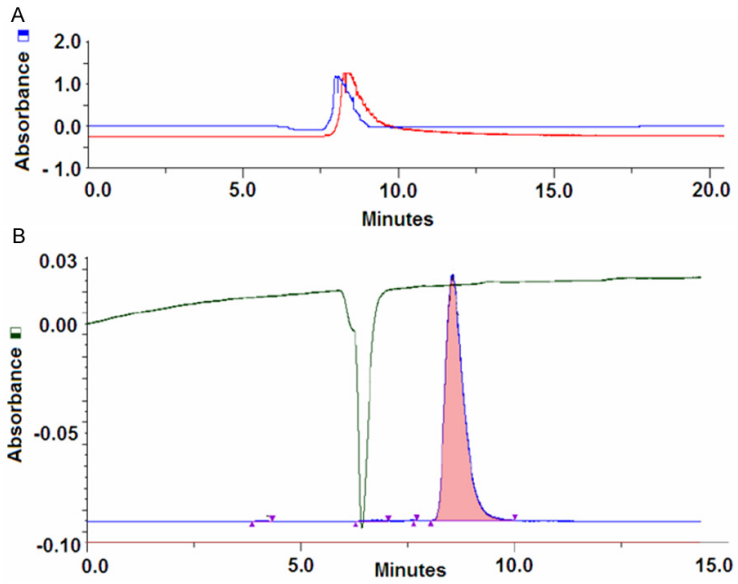

Figure 3. HPLC traces for the identity control (A) and the quality control (B) of the final product 6-[18F]FDF.

values for cumulated activity averaged at each time point. Standard errors of the means (SEM) were calculated for each mean value.

Results

Radiosynthesis of 6-[18F]FDF under GMP conditions

Automated radiosynthesis of 6-[18F]FDF using the Tracerlab FX_{FN} ASU is summarized in **Figure 2**.

In the first reaction step (**Figure 2**, R1), no-carrier added (n.c.a.) [18F]fluoride was removed from [18O]H_2O using a Chromafix Strong PS-DVB cartridge. The anion exchange resin efficiently retained radiofluoride while allowing passage of [18O]H_2O. A solution (0.8 mL) containing potassium carbonate (3.6 mg of K_2CO_3 in 0.2 mL H_2O) and Kryptofix 2.2.2 (14.5 mg in 0.6 mL CH_3CN) was used to elute n.c.a. [18F]fluoride from the resin (**Figure 2**; R1). The [18F]KF solution was azeotropically dried by the consecutive addition and removal of anhydrous CH_3CN. Initial azeotropic distillation was performed at 55°C for 1 min at 0.1 bar. Upon completion of the first evaporation step, an additional 1 mL of CH_3CN was added to reactor, and the solvents were evaporated at 55°C for 1 min at 0.1 bar followed by an evaporation step at 95°C for 3 minutes under high vacuum (0.01 bar). The end of the process yielded dried [18F]KF suitable for subsequent nucleophilic radiofluorination.

The second reaction step (**Figure 2**; R2) involved incorporation of n.c.a. [18F]KF into methyl 1,3,4-tri-*O*-acetyl-6-*O*-(methylbenzenesulfonyl)-α/β-D-fructofuranoside as the labeling precursor to afford intermediate 1. Radiofluorination was carried out in anhydrous CH_3CN (0.5 mL) using 7-14 mg of tosylate labeling precursor at 140°C for 20 min to give radiofluorinated 1-methyl tri-acetylated fructofuranoside as intermediate 1.

Final synthetis step (**Figure 2**; R3) involved acidic hydrolysis of intermediate 1 by adding 2N HCl (1 mL) to the reaction mixture. Treatment of intermediate 1 with 2N HCl rapidly hydrolyzed acetyl and methyl groups to yield the final product 6-[18F]FDF. The hydrolysis step was optimized with regard to acid strength and time to achieve high radiochemical yields within a short reaction time. Crude reaction mixture was diluted with 1 mL of 0.1 M sodium acetate buffer (pH = 5.4, (HPLC Purification Mobile Phase) and 2.0 mL of sterile water. This solution was filtered through a N-Alumina cartridge to remove [18F]fluoride prior to transfer into a collection vial for subsequent HPLC purification.

N-Alumina cartridge-based filtration of the crude reaction product obtained after the 3rd reaction step removed most of unreacted [18F]fluoride to facilitate the purification process using the HPLC system attached to the ASU. Crude reaction mixture was loaded onto a 5 mL injection loop. HPLC purification was carried out using a Phenomenex Nucleosil LUNA (II) RP C18 pre-column (5 μm, 50 x 10 mm) and Phenomenex Nucleosil Luna C18 column (10 μm, 250 x 10 mm) employing isocratic elution with 100% 0.1 M sodium acetate buffer (pH = 5.4) at a flow rate of 2 mL/min. Product peak was collected between 9.9 and 10.9 min. Collected peak (~2 mL) was transferred into a sterile vial through a sterile filter. The overall isolated radiochemical yield of 6-[18F]FDF was

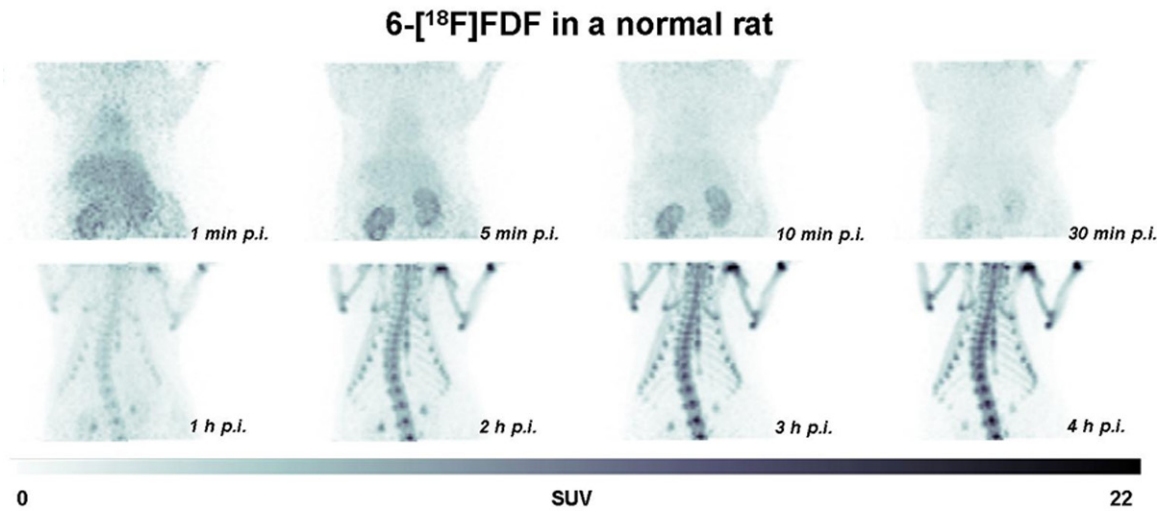

Figure 4. Selected PET images of a Sprague-Dawley rat at 1, 5, 20 and 30 min as well as 1, 2, 3 and 4 h p.i. of 12.15 MBq 6-[18F]FDF. Images are displayed as maximum intensity projections (MIPs).

14 ± 3% (n = 11, decay-corrected) at high radiochemical purity of greater than 95%.

Quality control of 6-[18F]FDF under GMP conditions

Identity of 6-[18F]FDF was confirmed by HPLC and radio-TLC using co-injection and co-spotting with reference compound, respectively. Representative HPLC-traces are given in **Figure 3A**. Quality control was carried out using a Gilson HPLC (Mandel Scientific Company Inc.; Guelph, Ontario, Canada) by injection of HPLC-purified 6-[18F]FDF onto a Phenomenex Nucleosil Luna C18 column (10 µm, 250 x 10 mm) and elution with 0.1 M sodium acetate buffer (pH = 5.4) at a flow rate of 2 mL/min (**Figure 3B**).

Radio-TLC analysis on silica-gel plates gave a R_f value of 0.6 in 95% CH_3CN/H_2O for 6-[18F]FDF. Specific activity of 6-[18F]FDF was assessed using UV absorption of cold 6-FDF. The UV detection limit for 6-FDF was determined to be 0.1 mg/ml. Based on the injected radioactivity amount, the minimum specific activity of 6-[18F]FDF was determined to be 5.1 GBq/µmol. However, exact specific activity of 6-[18F]FDF in the final product solution is higher, since the UV trace of the analytical HPLC at 220 nm showed no mass peak corresponding to unlabeled 6-FDF.

Subsequently, 6-[18F]FDF samples underwent a series of quality control tests according to the specification for clinical validation of radiopharmaceuticals as required by Health Canada including an appearance test, a stability test, a test for pH, a radionuclide identification test, a residual Kryptofix 222 test and finally the sterility and bacterial endotoxin test. The final 6-[18F]FDF solution ready for injections had a pH between 4.8 and 6 and was stable (> 95%) in saline for up to 12 h after radiosynthesis.

In vivo PET experiments

Radiolabeled fructose derivative 6-[18F]FDF was further evaluated *in vivo* in order to obtain estimates of human normal organ radiation doses required for a first study in man. **Figure 4** displays dynamic PET images of the abdominal part of a Sprague-Dawley rat after injection of 6-[18F]FDF at selected time points ranging from 1 min to 4 h p.i..

During the first 30 min after radiotracer injection, an initial circulation uptake and renal clearance pattern is observed with low background radioactivity in other organs. However, at 1 h p.i. and later time points, a continuous increase of radioactivity in bones was visible. **Figure 5** depicts extracted time-activity curves (TACs) for radioactivity uptake and clearance through the kidneys, the blood pool, liver, muscle tissue and bones. The radioactivity detected in bones shows an initial uptake which plateaued for about 30 min before a continuous increase was observed for to the rest of the PET imaging experiment.

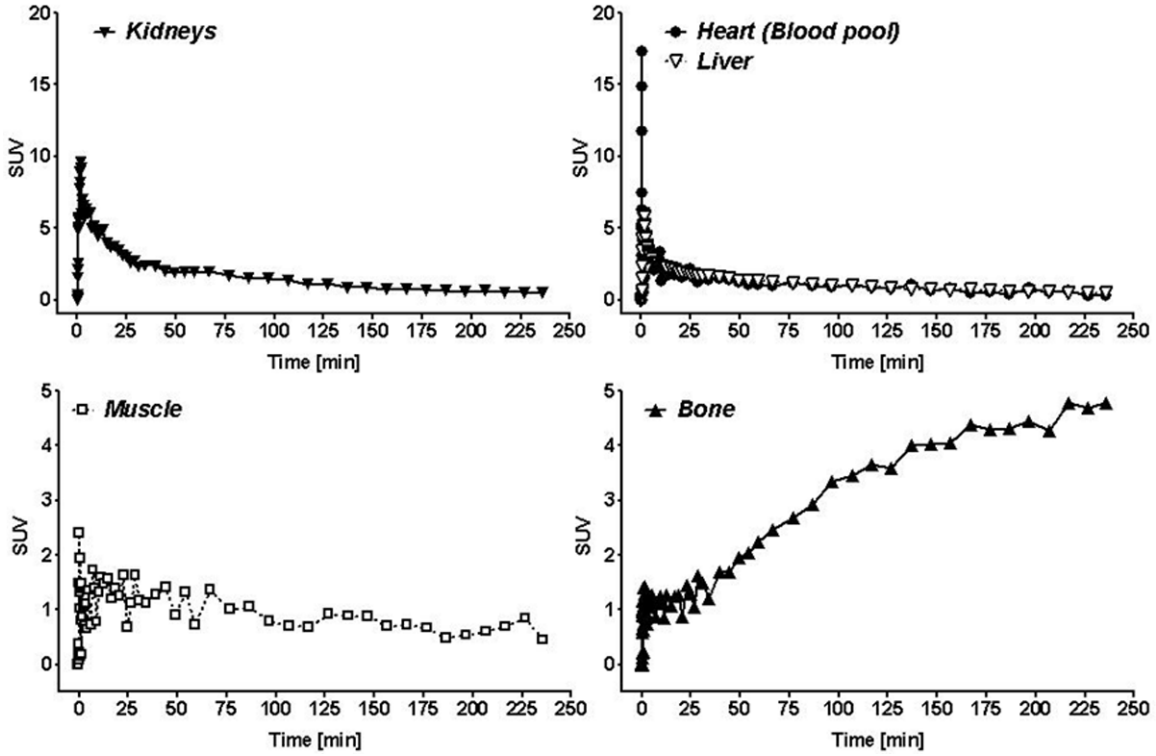

Figure 5. Time-activity curves (TACs) for heart (blood pool), liver, kidneys, muscle and bone derived from the dynamic PET experiment. Data are presented as SUV.

Biodistribution and dosimetry

For the dosimetry calculation a detailed *ex vivo* biodistribution experiment was carried out in rats at 5, 30 and 60 min as well as 2, 3, 4 and 6 h p.i. **Table 1** summarizes data biodistribution for 5, 60 min and 1, 2 and 6 h p.i. Except for bone and brain tissue all organs possessed a clearance pattern.

Table 2 presents the calculated human absorbed doses and effective dose for 6-[18F]FDF as determined using OLINDA/EXM.

The human effective whole body dose determination resulted in 0.0085 mSv/MBq and 0.010 mSv/MBq for the human adult male and female phantom. The highest absorbed doses resulted for the red marrow and osteogenic cells, corresponding to the high amounts of radioactivity detected with the PET experiments in the bones (**Figures 4** and **5**). For the osteogenic cells dose equivalents of 0.029 mSv/MBq and 0.038 mSv/MBq for a human male and female were calculated. An injected activity of 370 MBq (10 mCi) of 6-[18F]FDF would expose an adult human male to 3.1 mSv and a human male to 3.7 mSv effective radiation dose.

Discussion

This study presents the radiosynthesis of patient doses and human radiation dose calculations of 6-[18F]FDF, a novel 18F-labeled fructose derivative for imaging GLUT5 *in vivo*. Radiosynthesis of 6-[18F]FDF was accomplished in an automated synthesis unit under GMP conditions. Automated synthesis and dosimetry data of 6-[18F]FDF are important prerequisites for using the radiotracer in a first-in-human clinical study.

Radiosynthesis of 6-[18F]FDF was optimized using a tosylate labeling precursor instead of previously reported triflate precursor [20]. Tosylate labeling precursor offers several advantages such as its solid form and higher stability, which allows for a longer shelf life of up to 3 months without significant decomposition. A reliable and robust radiosynthesis of 6-[18F]FDF was developed in an ASU. The GE Tracerlab FX_{FN} ASU used in our study is fre-

Table 1. Biodistribution of 6-[18F]FDF in rats [%ID/g; n = 3]

Organs	5 min	1 hour	2 hours	6 hours
Blood	0.739 ± 0.011	0.398 ± 0.026	0.183 ± 0.026	0.034 ± 0.005
Heart	0.636 ± 0.011	0.303 ± 0.023	0.179 ± 0.046	0.029 ± 0.003
Lung	0.607 ± 0.040	0.322 ± 0.028	0.152 ± 0.023	0.037 ± 0.004
Liver	0.577 ± 0.009	0.347 ± 0.028	0.218 ± 0.051	0.064 ± 0.012
Kidneys	3.052 ± 0.300	0.875 ± 0.105	0.420 ± 0.078	0.064 ± 0.016
Thymus	0.489 ± 0.020	0.280 ± 0.032	0.156 ± 0.385	0.023 ± 0.002
Spleen	0.449 ± 0.013	0.284 ± 0.016	0.147 ± 0.005	0.053 ± 0.003
Duodenum	0.704 ± 0.011	0.327 ± 0.006	0.189 ± 0.021	0.051 ± 0.015
Small Intestine	0.627 ± 0.004	0.340 ± 0.009	0.236 ± 0.055	0.046 ± 0.010
Large Intestine	0.230 ± 0.005	0.279 ± 0.007	0.534 ± 0.218	0.495 ± 0.046
Pancreas	0.283 ± 0.015	0.179 ± 0.015	0.095 ± 0.016	0.024 ± 0.002
Bone	0.234 ± 0.025	0.795 ± 0.046	0.786 ± 0.344	0.094 ± 0.026
Muscle	0.240 ± 0.010	0.310 ± 0.024	0.156 ± 0.020	0.023 ± 0.003
Stomach	0.274 ± 0.090	0.245 ± 0.020	0.147 ± 0.027	0.020 ± 0.001
Ovaries	0.470 ± 0.064	0.323 ± 0.029	0.145 ± 0.042	0.025 ± 0.005
Brain	0.129 ± 0.016	0.240 ± 0.015	0.186 ± 0.005	0.043 ± 0.005
Bladder	0.831 ± 0.119	1.305 ± 0.171	1.095 ± 0.621	0.153 ± 0.044
Fat	0.077 ± 0.016	0.053 ± 0.009	0.016 ± 0.003	0.005 ± 0.001

quently employed as an effective synthesis module for automated radiosyntheses of numerous PET radiotracers for clinical applications such as [18F]FLT, [18F]FAZA, [18F]fluorocholine and [18F]FET [21]. 6-[18F]FDF could be prepared in decay-corrected radiochemical yields of ~14%. The minimum specific activity was determined to be 5.1 GBq/μmol. The high radiochemical (radiochemical purity > 95%) and chemical purity (no chemical contaminations visible in the UV trace of purified product), and the successful quality control tests make prepared 6-[18F]FDF suitable for injections into humans.

The highest absorbed doses are observed in bone forming cells, red marrow and osteogenic cells. This is consistent with findings from mouse and rat PET image analysis, where bone was found to possess the highest radioactivity levels at 1 h p.i. [20] followed by a further increase for up to 2 h. Higher radiation dose levels are also expected for the kidneys and urinary bladder since 6-[18F]FDF has shown mainly a renal clearance pattern.

The Food and Drug Administration's Radioactive Drug Research Committee (FDA-RDRC), in its Code of Federal Regulations 21CFR361.1 [22], limits the single dose of radiation to the whole body, active blood-forming organs, lens of the eye and gonads to 30 mSv and for other organs to 50 mSv. The data presented here indicates that an injected dose of 370 MBq (10 mCi), based on a typical prescribed dose of 5.2 MBq/kg for FDG [26], would not exceed these limits. The critical organs, i.e. osteogenic cells and red bone marrow, would absorb 11.7 and 4.4 mSv in this case. The effective whole body dose to a human determined from this investigation is 0.0089 mSv/MBq. This value compares favorably with the one reported for FDG in the SNM procedure guidelines of 0.027 mSv/MBq [27] and the ICRP of 0.019 mSv/MBq [28].

To date [18F]FDG is still the most widely used PET radiotracer, being used in > 90% of all PET studies, and it has proven its usefulness for diagnosis, staging and detection of residual/recurrent cancer [29]. However, [18F]FDG displays some important limitations for tumor detection including uptake into inflammatory lesions which might confound the adequate differentiation between post-therapy inflammation and residual tumor [30, 31]. In breast cancer patients, [18F]FDG-PET has been shown to possess a 76-89% sensitivity and 73-80% specificity for the primary diagnosis. It shows, however, only low and very variable sensitivity of 20-50% to detect axillary lymph node metastasis [12]. The shortcomings of [18F]FDG have led to the development of alternative PET and

Table 2. Predicted human absorbed doses for 6-[18F]FDF

Organs	Absorbed dose [mGv/MBq]
Adrenals	0.0069
Brain	0.0051
Breasts	0.0037
Gallbladder wall	0.0074
Lower low intestine wall	0.0118
Small intestine	0.0151
Stomach wall	0.0060
Upper low intestine wall	0.0117
Heart wall	0.0075
Kidneys	0.0202
Liver	0.0132
Lungs	0.0059
Muscle	0.0055
Ovaries	0.0092
Pancreas	0.0065
Red marrow	0.0119
Osteogenic cells	0.0315
Skin	0.0036
Spleen	0.0063
Testes	0.0045
Thymus	0.0049
Thyroid	0.0048
Urinary bladder wall	0.0179
Uterus	0.0073
Total body	0.0071
Effective dose	0.0089 mSv/MBq
Effective dose equivalent	0.0108 mSv/MBq

SPECT radiotracers using different targeting approaches [15]. Fructose and analogues may become molecules of interest to study tumor growth and metabolic syndrome [32]. Fructose transport through GLUT5, which is expressed in breast cancer, would represent an alternative targeting strategy [33]. Although Gambhir and co-workers have recently raised questions about the degree of overexpression of GLUT5 in human breast cancer tissue [15], it remains to be elucidated whether there would be a functional difference in fructose and glucose metabolism in breast cancer patients with different types of breast tumors. It was found earlier that D-fructose is taken up to significantly higher degrees in breast cancer cells compared to a non-tumorigenic epithelial cell line [12]. Uptake via fructose transporting GLUTs has been assessed earlier by 1-[18F]FDF [16]. It was demonstrated that 1-[18F]FDF showed no selective uptake in GLUT5 expressing tissue, whereas 6-[18F]FDF showed selective uptake into GLUT5 expressing tissue, specifically breast cancer cells [32]. This finding and the favorable radiopharmacological profile of 6-[18F]FDF in various murine and human breast cancer cell lines suggest application of 6-[18F]FDF for imaging of GLUT5 in breast cancer patients [19, 20]. An interesting pharmacological aspect of 6-[18F]FDF is the observed bone uptake ([20]; current study). According to the obtained time-activity curves in bone, radioactivity accumulation seems to occur in two phases: a) an initial uptake during the first 30 min followed by b) an increased uptake starting at 30 min p.i. until the end of the study at 4 h p.i. The observed time-activity curve is atypical for a sole radiodefluorination process. Bone uptake levels are significantly higher and differ markedly in the uptake kinetics after injection of [18F]fluoride [unpublished data]. There is initial evidence that GLUT5 is expressed in chondrozytes suggesting a role for fructose transport and metabolism during the synthesis and degradation of cartilage [34, 35]. However, detailed function of proposed GLUT5 expression in chondrocytes is still not fully understood, but it is not a limiting factor for the application of 6-[18F]FDF as PET radiotracer for molecular imaging of GLUT5 in breast cancer.

In conclusion, the pre-clinical evaluation in different models of breast cancer revealed that 6-[18F]FDF shows significant levels of uptake in breast cancer tissue and a fast clearance leading to low background levels which would be favorable for a PET radiotracer. Moreover, favorable dosimetry data for 6-[18F]FDF and its advantageous clearance properties, other than the observed accumulation in bone, would support further testing of 6-[18F]FDF as a new PET radiotracer in a first human clinical study.

Acknowledgements

The authors would like to thank Dr. John Wilson, David Clendening and Blake Lazurko from the Edmonton PET Center for providing 18F produced on a biomedical cyclotron and Monica Wang and Brendan J. Trayner for helping with the biodistribution experiment. This work was funded by grants from the Canadian Breast Cancer Foundation (CBCF RES0000024), Canadian Institutes of Health Research (CIHR

CPG 365459-2009) and the Natural Sciences and Engineering Research Council (NSERC CHRPJ 365459-2009).

Disclosure of conflict of interest

The authors declare they have no conflicts of interest.

Address correspondence to: Dr. Frank Wuest, Department of Oncology, Cross Cancer Institute, 11560 University Ave, Edmonton, Alberta, Canada T6G 1Z2. E-mail: wuest@ualberta.ca

References

[1] Redig AJ, McAllister SS. Breast cancer as a systemic disease: a view of metastasis. J Intern Med 2013; 274: 113-26.

[2] Debergh I, Vanhove C, Ceelen W. Innovation in cancer imaging. Eur Surg Res 2012; 48: 121-30.

[3] Groheux D, Espié M, Giacchetti S, Hindié E. Performance of FDG PET/CT in the clinical management of breast cancer. Radiology 2013; 266: 388-405.

[4] Cintolo JA, Tchou J, Pryma DA. Diagnostic and prognostic application of positron emission tomography in breast imaging: emerging uses and the role of PET in monitoring treatment response. Breast Cancer Res Treat 2013; 138: 331-46.

[5] Macheda ML, Rogers S, Best JD. Molecular and cellular regulation of glucose transporter (GLUT) proteins in cancer. J Cell Physiol 2005; 202: 654-62.

[6] Krzeslak A, Wojcik-Krowiranda K, Forma E, Jozwiak P, Romanowicz H, Bienkiewicz A, Brys M. Expression of GLUT1 and GLUT3 Glucose Transporters in Endometrial and Breast Cancers. Pathol Oncol Res 2012; 18: 721-28.

[7] Pinheiro C, Sousa B, Albergaria A, Paredes J, Dufloth R, Vieira D, Schmitt F, Baltazar F. GLUT1 and CAIX expression profiles in breast cancer correlate with adverse prognostic factors and MCT1 overexpression. Histol Histopathol 2011; 26: 1279-86.

[8] Vermeulen JF, van der Wall E, Witkamp AJ, van Diest PJ. Analysis of expression of membrane-bound tumor markers in ductal carcinoma in situ of the breast: paving the way for molecular imaging. Cell Oncol (Dordr) 2013; 36: 333-40.

[9] Buck AK, Schirrmeister H, Mattfeldt T, Reske SN. Biological characterisation of breast cancer by means of PET. Eur J Nucl Med Mol Imaging 2004; 31 Suppl 1: S80-S87.

[10] Sundararajan L, Linden HM, Link JM, Krohn KA, Mankoff DA. 18F-Fluoroestradiol. Semin Nucl Med 2007; 37: 460-6.

[11] Dehdashti F, McGuire AH, Van Brocklin HF, Siegel BA, Andriole DP, Griffeth LK, Pomper MG, Katzenellenbogen JA, Welch MJ. Assessment of 21-[18F]fluoro-16 alpha-ethyl-19-norprogesterone as a positron-emitting radiopharmaceutical for the detection of progestin receptors in human breast carcinomas. J Nucl Med 1991; 32: 1532-7.

[12] Lee JH, Zhou HB, Dence CS, Carlson KE, Welch MJ, Katzenellenbogen JA. Development of [F-18]fluorine-substituted Tanaproget as a progesterone receptor imaging agent for positron emission tomography. Bioconjug Chem 2010; 21: 1096-104.

[13] Zamora-León SP, Golde DW, Concha II, Rivas CI, Delgado-López F, Baselga J, Nualart F, Vera JC. Expression of the fructose transporter GLUT5 in human breast cancer. Proc Natl Acad Sci U S A 1996; 93: 1847-52.

[14] Godoy A, Ulloa V, Rodriguez F, Reinicke K, Yanez AJ, García Mde L, Medina RA, Carrasco M, Barberis S, Castro T, Martínez F, Koch X, Vera JC, Poblete MT, Figueroa CD, Peruzzo B, Pérez F, Nualart F. Differential subcellular distribution of glucose transporters GLUT1-6 and GLUT9 in human cancer: ultrastructural localization of GLUT1 and GLUT5 in breast tumor tissues. J Cell Physiol 2006; 207: 614-27.

[15] Gowrishankar G, Zitzmann-Kolbe S, Junutula A, Reeves R, Levi J, Srinivasan A, Bruus-Jensen K, Cyr J, Dinkelborg L, Gambhir SS. GLUT 5 is not over-expressed in breast cancer cells and patient breast cancer tissues. PLoS One 2011; 6: e26902.

[16] Haradahira T, Tanaka A, Maeda M, Kanazawa Y, Ichiya YI, Masuda K. Radiosynthesis, rodent biodistribution, and metabolism of 1-deoxy-1-[18F]fluoro-D-fructose. Nucl Med Biol 1995; 22: 719-25.

[17] Tatibouët A, Yang J, Morin C, Holman GD. Synthesis and evaluation of fructose analogues as inhibitors of the D-fructose transporter GLUT5. Bioorg Med Chem 2000; 8: 1825-33.

[18] Yang J, Dowden J, Tatibouët A, Hatanaka Y, Holman GD. Development of high-affinity ligands and photoaffinity labels for the D-fructose transporter GLUT5. Biochem J 2002; 367: 533-9.

[19] Trayner BJ, Grant TN, West FG, Cheeseman CI. Synthesis and characterization of 6-deoxy-6-fluoro-D-fructose as a potential compound for imaging breast cancer with PET. Bioorg Med Chem 2009; 17: 5488-95.

[20] Wuest M, Trayner BJ, Grant TN, Jans HS, Mercer JR, Murray D, West FG, McEwan A, Wuest F, Cheeseman CI. Radiopharmacological evaluation of 6-deoxy-6-[18F]fluoro-D-fructose as a radiotracer for PET imaging of GLUT5 in breast cancer. Nucl Med Biol 2011; 38: 461-75.

[21] Shao X, Hoareau R, Hockley BG, Tluczek LJ, Henderson BD, Padgett HC, Scott PJ. Highlighting the Versatility of the Tracerlab Synthesis Modules. Part 1: Fully Automated Production of [F]Labelled Radiopharmaceuticals using a Tracerlab FX(FN). J Labelled Comp Radiopharm 2011; 54: 292-307.
[22] Guidance for Industry, investigators and reviewers: exploratory IND studies. U.S. Food and Drug Administration. 2006.
[23] Stabin MG, Sparks RB, Crowe E. OLINDA/EXM: the second-generation personal computer software for internal dose assessment in nuclear medicine. J Nucl Med 2005; 46: 1023-7.
[24] Basic anatomical and physiological data for use in radiological protection: reference values. A report of age- and gender-related differences in the anatomical and physiological characteristics of reference individuals. ICRP Publication 89. Ann ICRP 2002; 32: 5-265.
[25] Stabin M, Emmons MA, Segars WP, Fernald M and Brill AB. ICRP-89 based adult and pediatric phantom series. J Nucl Med 2008; 49 Suppl 1: 14P.
[26] Abdele JT, Fung CI. Effect of hepatic steatosis on liver FDG uptake measured in mean standard uptake values. Radiology 2010; 254: 917-24.
[27] Prescription drugs for human use generally recognized as safe and effective and not misbranded: drugs used in research; Sec. 361.1 Radioactive drugs for certain research uses, Code of Federal Regulations Title 21, 21CFR361, 1.
[28] Radiation dose to patients from radiopharmaceuticals. ICRP Publication 106. Ann ICRP 2007; 38: 1-2.
[29] Fleming IN, Gilbert FJ, Miles KA, Cameron D. Opportunities for PET to deliver clinical benefit in cancer: breast cancer as a paradigm. Cancer Imaging 2010; 10: 144-52.
[30] Shreve PD, Anzai Y, Wahl RL. Pitfalls in oncologic diagnosis with FDG PET imaging: physiologic and benign variants. Radiographics 1999; 19: 61-77.
[31] Belhocine T, Spaepen K, Dusart M, Castaigne C, Muylle K, Bourgeois P, Bourgeois D, Dierickx L, Flamen P. 18FDG PET in oncology: the best and the worst. Int J Oncol 2006; 28: 1249-61.
[32] Tanasova M, Plutschak M, Muroski ME, Sturla SJ, Strouse GF, McQuade DT. Fluorescent THF-based fructose analogue exhibits fructose-dependent uptake. Chem Bio Chem 2013; 14: 1263-70.
[33] Levi J, Cheng Z, Gheysens O, Patel M, Chan CT, Wang Y, Namavari M, Gambhir SS. Fluorescent fructose derivatives for imaging breast cancer cells. Bioconjug Chem 2007; 18: 628-34.
[34] Ohara H, Tamayama T, Maemura K, Kanbara K, Hayasaki H, Abe M, Watanabe M. Immunocytochemical demonstration of glucose transporters in epiphyseal growth plate chondrocytes of young rats in correlation with autoradiographic distribution of 2-deoxyglucose in chondrocytes of mice. Acta Histochem 2001; 103: 365-78.
[35] Richardson S, Neama G, Phillips T, Bell S, Carter SD, Moley KH, Moley JF, Vannucci SJ, Mobasheri A. Molecular characterization and partial cDNA cloning of facilitative glucose transporters expressed in human articular chondrocytes; stimulation of 2-deoxyglucose uptake by IGF-I and elevated MMP-2 secretion by glucose deprivation. Osteoarthritis Cartilage 2003; 11: 92-101.